RSC Advances

ROYAL SOCIETY OF CHEMISTRY

www.rsc.org/advances

Controllable Synthesis of Phosphate-modified $BiPO_4$ Nanorods with High Photocatalytic Activity: Surface Hydroxyl Groups Concentrations Effects

Yan Li[a,b], Yawen Wang[a,*], Yu Huang[b,c,*], Junji Cao[b,c], Wingkei Ho[d], Shuncheng Lee[e], Caimei Fan[a]

[a] *College of Chemistry and Chemical Engineering, Taiyuan University of Technology, Taiyuan 030024, China*

[b] *Key Lab of Aerosol Chemistry & Physics，Institute of Earth Environment, Chinese Academy of Sciences, Xi'an 710075, China*

[c] *State Key Lab of Loess and Quaternary Geology (SKLLQG), Institute of Earth Environment, Chinese Academy of Sciences, Xi'an 710075, China*

[d] *Department of Science and Environmental Studies, The Hong Kong Institute of Education, Tai Po, New Territories, Hong Kong*

[e] *Department of Civil and Environmental Engineering, The Hong Kong Polytechnic University, Hung Hom, Hong Kong*

**Corresponding author:*

E-mail address: wangyawen@tyut.edu.cn (Dr. Yawen Wang), huangyu@ieecas.cn (Prof. Yu Huang)

Tel: 86-29-6233 6261

Abstract:

Surface property of photocatalysts is crucial to improve their removal efficiency of wastewater pollutants. In this study, phosphate-modified $BiPO_4$ photocatalysts with different PO_4^{3-}/Bi molar ratios were controllably synthesized through a one-pot hydrothermal method. The surface hydroxyl groups concentrations of $BiPO_4$ samples can be tuned by adjusting the PO_4^{3-}/ Bi^{3+} molar ratios. XRD results showed that surface modification by phosphate could boost the crystallinity of $BiPO_4$, which was beneficial to photocatalytic performance. XPS and IR spectra revealed that PO_4^{3-} modified only on the surface of $BiPO_4$. The optical absorption of phosphate-modified $BiPO_4$ samples showed obvious blue shift compared with that of bare $BiPO_4$. Photocatalytic activities of the as-prepared samples were evaluated by the decomposition of methylene orange (MO) under ultraviolet light and simulated solar-light irradiation, respectively. Experimental results demonstrated that the photocatalytic performance of the modified samples significantly improved after $BiPO_4$ surface was modified by different amounts of PO_4^{3-}. Both indirect scavenger method and electron spin resonance method were adopted to determine the production and intensity of free radicals during photocatalytic degradation. Results suggested that MO was predominantly removed through oxidation by OH radicals, as confirmed by theoretical calculations. Moreover, the photocatalytic degradation mechanism of MO over as-prepared phosphate-modified $BiPO_4$ was proposed.

Keywords:

Surface modification; phosphate; $BiPO_4$; electron spin resonance (ESR) method; photocatalysis

1. Introduction

Water pollution by organic pollutants such as dyes is a serious environmental problem for human society; the pollutants must be removed or eliminated to an acceptable level before water is discharged into the natural environment [1]. Among various dye wastewater treatment techniques, photocatalysis has attracted more and more attention because of its ability to mineralize organic pollutants by absorbing solar light [2]. TiO_2, has good stability and low cost; thus, this material is considered an attractive photocatalyst of dye degradation. Nevertheless, the photocatalytic activity of TiO_2 is not high enough for industrial purposes, because of the limitations of the absorption edge and the recombination of photogenerated charges [3, 4]. Therefore, several efforts have been made to develop novel semiconductor photocatalysts or to modify traditional photocatalysts to overcome the drawbacks of TiO_2 achieve the maximum activity [5-7].

$BiPO_4$ photocatalyst, was first reported by Zhu's group [4] in a study on the degradation of methylene blue (MB). This photocatalyst showed superior activity compared with commercial P25. Henceforth, $BiPO_4$ and its derivatives have been intensively investigated for the degradation of abundant pollutants, such as methyl orange (MO) [8-10], rhodamine B (RhB) [2, 11, 12], methyl blue (MB) [13-15], phenol [16, 17], benzene [18], carbamazepine [19] and so on. Moreover, $BiPO_4$ has been applied in catalysis, ion sensing, radioactive element separation and humidity sensing [20-23]. Given its larger dipole moments, monoclinic $BiPO_4$ (space group: P21/n) exhibited superior activity over the two other crystal phases of $BiPO_4$: hexagon (space group: $P3_123$) and monoclinic (space group: P21/m) [14]. However, the significant combination of photo-generated charge carriers produces the low quantum efficiency of $BiPO_4$ photocatalysts. Therefore, various studies have been conducted to improve the electron–hole separation efficiency of $BiPO_4$. For example, the construction of heterojunction interfaces between $BiPO_4$ and other semiconductors can facilitate the separation and transfer of photogenerated electron–hole pairs [23,

24]. Precious metal deposits can accelerate the migration of generated electrons from $BiPO_4$ to metal particles, which prolongs the lifetime of a hole to enhance the $BiPO_4$ activity [25]. Nonmetal doping such as F-doping can increase the polarizability, whereas N-doping can decrease the electric resistance [26, 27]; all these will eventually result in high photocatalytic activity. Meanwhile, Ag-doped $BiPO_4$ is a product of metal doping that can enhance the electron hole separation by changing the $BiPO_4$ morphology and size, thereby promoting its anisotropic carrier transport [11]. In addition to the traditional methods, a study of surface modification carried out by Pan et al. [2] showed that the OH groups on the $BiPO_4$ surface can efficiently restrain the combination rate of photogenerated electron–hole pairs by forming •OH radicals. In addition, Lv et al. [28, 29] found that the broadening of the valence band (VB) induced by surface oxygen-vacancy states can enhance the high separation efficiency of photoinduced electron–hole pairs.

Moreover, surface modification is an alternative method to enhance the photocatalytic performance of semiconductor photocatalysts. Inorganic oxyanions such as phosphate (PO_4^{3-}) are known to be strongly adsorbed on the surface of semiconductors; these ions greatly influence the interfacial and surface chemistry [30-31]. A previous study showed that phosphate surface modification over TiO_2 can largely accelerate the hydroxyl radical attack and hinder the direct hole oxidation pathway [33]. Modifications with PO_4^{3-} can also promote O_2 adsorption which prolongs the lifetime and enhances the separation of the photo-generated charge carriers of the resulting products [30, 34, 35]. These results demonstrated that PO_4^{3-} definitely has an influence on the catalytic properties of photocatalysts, which is attributed to its sufficient efficiency for electron–hole separation. To the best of our knowledge, the surface modification of $BiPO_4$ by phosphate has been mentioned and predicted [4, 36], but its related influence on the photocatalytic performance has not been previously reported. Therefore, the potential effects of phosphate surface modification on the physical and chemical properties of $BiPO_4$ should be explored.

In this work, surface-modified $BiPO_4$ by phosphate was synthesized by a one-pot hydrothermal method. The effect of the surface medication by phosphate on the photocatalytic performance of $BiPO_4$ was elucidated in detail.

2. Experimental

2.1. Synthesis of bare $BiPO_4$ and phosphate-modified $BiPO_4$ samples

All solvents and reagents are of analytical grade and directly used without further purification. $BiPO_4$ and phosphate-modified $BiPO_4$ were synthesized by the hydrothermal method, with $Bi(NO_3)_3{\cdot}5H_2O$ and $NaH_2PO_4{\cdot}2H_2O$ as precursors. In a typical procedure, 1 mmol of $Bi(NO_3)_3{\cdot}5H_2O$ and different amounts of $NaH_2PO_4{\cdot}2H_2O$ were dissolved in 15 mL of deionized water under vigorous stirring for 1 h. The mixture was transferred to a Teflon-lined stainless steel autoclave (20 mL capacity) and maintained at 160 °C for 24 h. The as-prepared samples were collected by centrifugation, washed several times with deionized water, and dried at 60 °C in an oven. For the synthesis of bare $BiPO_4$ (denoted as $BP_{1.0}$), the molar ratios of $NaH_2PO_4{\cdot}2H_2O$ to $Bi(NO_3)_3{\cdot}5H_2O$ were controlled at 1.0. For the synthesis of phosphate-modified $BiPO_4$ samples, the molar ratios of $NaH_2PO_4{\cdot}2H_2O$ to $Bi(NO_3)_3{\cdot}5H_2O$ were controlled at 1.1, 1.3, and 1.5, and the corresponding products were denoted as $BP_{1.1}$, $BP_{1.3}$, and $BP_{1.5}$, respectively.

2.2. Characterization

Various methods were used to characterize the physical and chemical properties of the as-prepared bare $BiPO_4$ and phosphate-modified $BiPO_4$ samples. The X-ray powder diffraction (XRD) patterns were recorded on a PANalytical XPert PRO X-ray diffractometer system with Cu Kα radiation (λ = 1.54178 Å) at a scan rate of 0.05° 2θ/s. The accelerating voltage and the applied current were 40 kV and 30 mA, respectively. Scanning electron microscopy (SEM; JEOL JSM-6490) was used to characterize the morphology of the obtained products. Transmission electron

microscopy (TEM) was performed with a JEOL JEM-2100HR CM-120 transmission electron microscope. The samples for TEM were prepared by dispersing the final powders in ethanol. The dispersion was then dropped on carbon copper grids. After the sample was vacuum-dried overnight at 573 K, the nitrogen adsorption and desorption isotherm at 77 K was measured by a Micrometritics ASAP2010 system. A Varian Cary 100 Scan UV-Visible system equipped with a labsphere diffuse reflectance accessory was used to obtain the reflectance spectra of the catalysts over a range of 200–800 nm. Labsphere USRS-99-010 was employed as a reflectance standard. The spectra were converted from reflection to absorbance by the Kubelka–Munk method. X-ray photoelectron spectroscopy (XPS) measurements were performed with an X-ray photoelectron spectrometer (Thermo ESCALAB 250). All the binding energies were calibrated to the C 1*s* peak at 284.8 eV of the surface adventitious carbon. The Fourier transform infrared spectroscopy (FTIR) spectra were recorded on a FTIR absorption spectrometer (Magna-IR 750, Nicolet, USA), with KBr as the diluent. Photoluminescence (PL; F-7000, Hitachi, Japan) was used to investigate the optical properties of the as-prepared samples. The samples for electron spin-resonance spectroscopy (ESR; ER200-SRC, Bruker, Germany) were prepared by mixing 0.05 g of the as-prepared photocatalyst in a 25 mM 5,5'-dimethyl-1-pirroline-*N*-oxide (DMPO) solution with a 50 mL aqueous dispersion for DMPO–•OH or a 50 mL alcohol dispersion for DMPO–•O_2^-, respectively, under irradiation with 254 nm ultraviolet (UV) light.

2.3 Photoelectrochemical measurements

The photoelectrochemical properties of $BP_{1.0}$ and $BP_{1.3}$ were evaluated using a Parstat 4000 electrochemical workstation (USA) in a conventional three-electrode cell, in which a platinum plate and Ag/AgCl electrode were used as counter electrode and reference electrode, respectively. In order to fabricate the working electrode, ethyl cellulose and terpineol were added into $BiPO_4$, which were then dispersed into ethanol to obtain homogeneous suspension through bath sonication. Then, $BiPO_4$

films were modified onto the fluorine doped tin oxide (FTO) conducting glass by dip coating and dried at room temperature. The final films on FTO were composed of 0.18 wt% $BiPO_4$, 0.09 wt% ethyl cellulose, and 0.73 wt% terpineol. Afterwards, the electrodes were heat-treated in a furnace at 500 ^oC for 30 min to remove the additives. The current-time curves were measured at 0.0 V vs. Ag/AgCl in 0.1 mol/L Na_2SO_3 at ambient temperature under the irradiation of a 300 W Xenon lamp.

2.4. Photocatalytic activity test

The photocatalytic activities of bare $BiPO_4$ and phosphate-modified $BiPO_4$ samples were evaluated by the degradation of methyl orange (MO) under ultraviolet light and simulated solar-light irradiation, respectively. Briefly, 0.05 g of the as-prepared photocatalyst was added to 50 mL of 5 mg/L MO aqueous solution in a container with a cooling water jacket. The temperature of the solution during the photodegradation was kept at approximately 25 °C. The MO solution with the photocatalyst was continuously stirred for 1 h to ensure the establishment of an adsorption–desorption equilibrium among the photocatalyst, MO, and water before the lamp was turned on. During the degradation, the MO solution with the photocatalyst was continuously stirred by a dynamoelectric stirrer. The concentration of MO was monitored by colorimetry with a U-3310 UV-Vis spectrometer (Hitachi) at fixed time intervals. The degradation rate of the MO solution after irradiation was calculated according to the following equation:

$$R = (A_0 - A_t) / A_0 \times 100\%$$

Where R is the degradation rate, A_0 is the absorbance of solution before irradiation, and A_t is the absorbance of solution in different periods after irradiation.

3. Results and discussion

3.1 XRD patterns of the as-prepared photocatalysts

Figure 1 shows the XRD patterns of the as-prepared bare $BiPO_4$ and phosphate-modified $BiPO_4$ samples. As shown in Figure 1, the XRD patterns of all the as-prepared $BiPO_4$ samples can be readily indexed as monoclinic $BiPO_4$ (JCPDS

no. 80-209) with a space group of P21/n (No. 14) and lattice constants of a = 6.762 Å, b = 6.951 Å, and c = 6.482 Å. No impurity peaks were observed in these patterns, thereby indicating the high purity of the products. The intense and sharp diffraction peaks suggested that the as-synthesized products were well crystallized. The intensity of the diffraction peaks clearly become stronger with increased PO_4^{3-} concentration until the molar ratio of PO_4^{3-} to Bi reached 1.5, thereby demonstrating that the surface modification by phosphate could boost the crystallinity of $BiPO_4$. This change is beneficial to photocatalytic performance because high crystallinity generally means fewer traps and stronger photocatalytic activity [37].

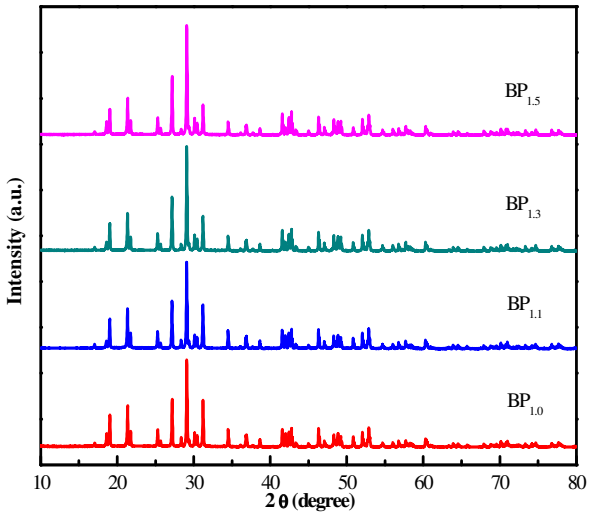

Fig. 1. XRD Patterns of the as-prepared bare $BiPO_4$ ($BP_{1.0}$) and phosphate-modified $BiPO_4$ ($BP_{1.1}$, $BP_{1.3}$, and $BP_{1.5}$) samples.

3.2 SEM

Figure 2 depicts typical SEM images of the as-prepared bare $BiPO_4$ and phosphate-modified $BiPO_4$ photocatalysts. With increased PO_4^{3-}/Bi^{3+} molar ratio during material synthesis, the morphology and particle size of the products significantly varied. When the PO_4^{3-}/Bi^{3+} molar ratio was equal to 1.0, the bare $BiPO_4$ ($BP_{1.0,}$ Figure 2a) sample was composed of irregular octahedral crystals with the sizes of approximately 1–2 μm. When the PO_4^{3-}/Bi^{3+} molar ratio varied from 1.1 to 1.5, the

morphology of the products became much more uniform. These products predominantly consisted of nanorods with diameters of approximately 200 nm and lengths of 1 μm, as shown in Figures 2b–2d. This trend revealed that the surface modification by PO_4^{3-} could hinder the growth of $BiPO_4$ crystals. The crystal structure had a tendency to be more perfect and have fewer defects, which is consistent with the XRD results. These uniform nanorods are beneficial to the improvement of photocatalytic performance.

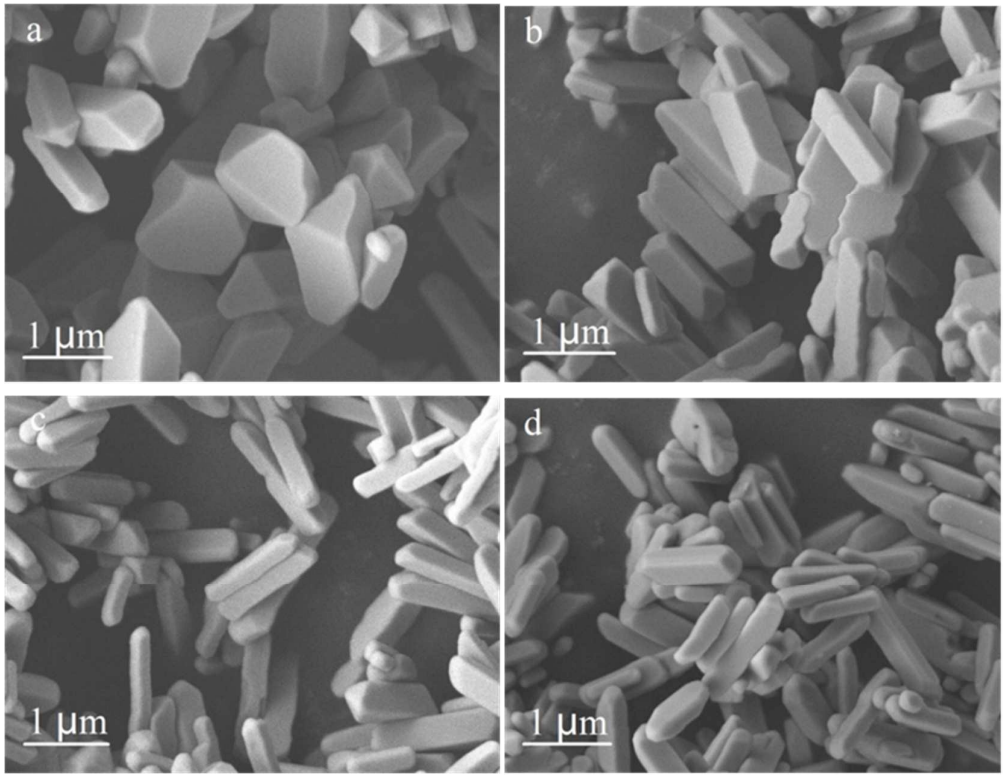

Fig. 2. SEM micrographs of the as-prepared products: (a) $BP_{1.0}$, (b) $BP_{1.1}$, (c) $BP_{1.3}$ and (d) $BP_{1.5}$.

3.3 TEM

Figure 3 presents the TEM characterization results of the as-prepared $BP_{1.0}$ and $BP_{1.3}$ samples. The TEM results are consistent with those of SEM (Figures 3a and 3b). As displayed in Figure 3a and 3b, the $BP_{1.0}$ sample was composed of irregular crystals with sizes of approximately 1–2 μm, whereas $BP_{1.3}$ was composed of uniform nanorods and microrods (with diameters of 200 nm and lengths of 1 μm), thereby

confirming the SEM characterization results. From Figures 3c and 3d, the clear lattice fringes with *d*-spacing of 0.323 and 0.469 nm were corresponding to the (200) plane of $BP_{1.0}$ and the (011) plane of $BP_{1.3}$, respectively. The corresponding SAED patterns (Figure 3e and 3f) showed clear diffraction spots, thereby indicating that the as-prepared samples are of a single crystalline phase.

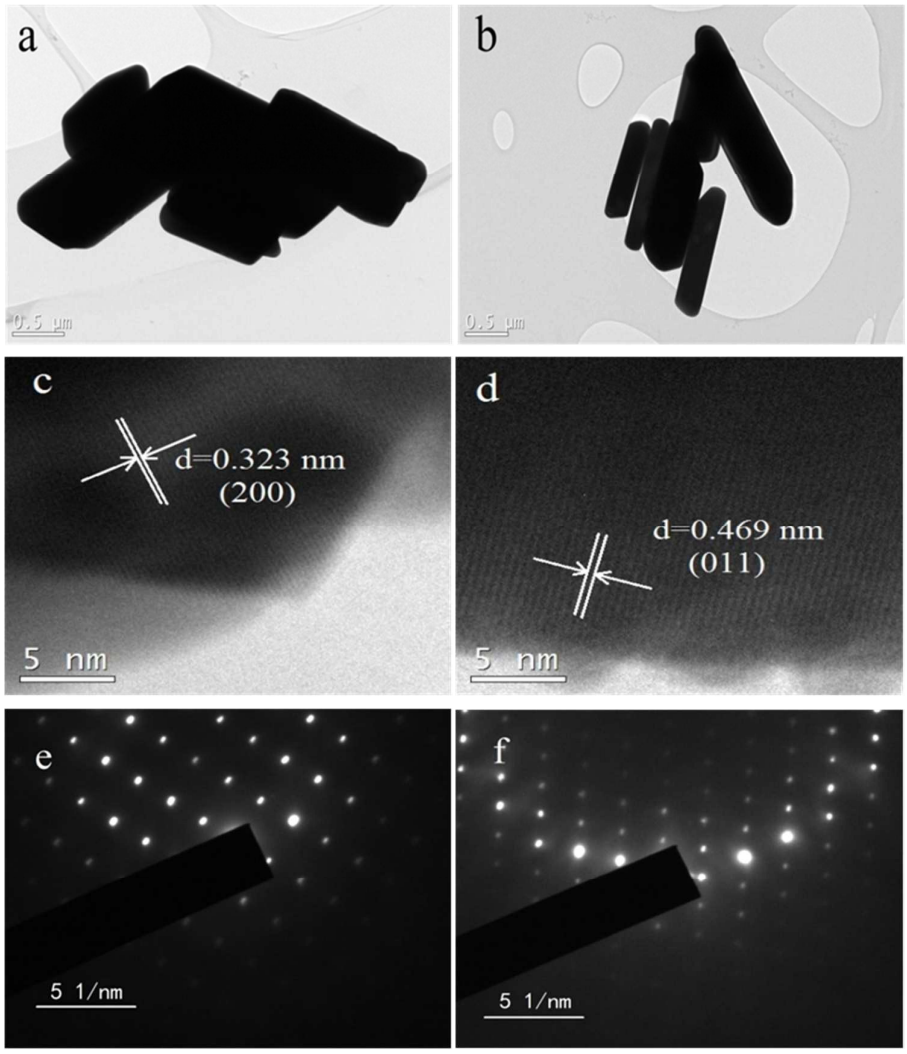

Fig. 3. TEM images: (a, b) low-magnification TEM images, (c, d) HR-TEM images and (e, f) SAED patterns of $BP_{1.0}$ and $BP_{1.3}$, respectively.

Given the SEM and TEM results, when the PO_4^{3-}/Bi^{3+} molar ratio varied from 1.0 to 1.5, the morphologies of the final products became more and more uniform while the particle size decreased accordingly. This trend can be ascribed to the electrostatic

repulsion of excess PO_4^{3-} on the surface of $BiPO_4$ during the crystal growth processes. The combination rate of the photo-excited electrons and holes is well known to have an important role in the improvement of the photocatalytic activity of the final products. Therefore, the phosphate-modified $BiPO_4$ nanorods with high crystallinity tend to have superior photocatalytic activity because of the high separation efficiencies of electrons and holes, which eventually facilitates the generation of active species.

3.4 FTIR spectra

The surface properties of bare $BiPO_4$ and phosphate-modified $BiPO_4$ samples were characterized by FTIR. As shown in Figure 4, the vibrations of peaks at 550, 850, 1000, and 1100 cm^{-1} are the characteristic ν1, ν2, ν3, and ν4 vibrations of PO_4^{3-} from $BiPO_4$ [2], respectively. The peaks at 1300–1400 cm^{-1} can be assigned to the characteristic frequencies of phosphoryl bonds (P=O); their gradually enhanced intensity suggested the presence of PO_4^{3-}. The surface PO_4^{3-} concentration increased as the PO_4^{3-}/Bi^{3+} molar ratio varied from 1.0 to 1.5 [38-40]. The broad peaks at 3480 and 1630 cm^{-1} are related to the hydroxyl stretching vibration of surface-adsorbed water and hydroxyl groups, respectively [41]. Obviously, the surface modification of $BiPO_4$ by PO_4^{3-} increased the concentrations of surface hydroxyl groups significantly as shown in Figure 4. Previous studies also showed that PO_4^{3-} has strong interaction with H_2O through hydrogen bond and exhibit strong binding affinity to the surface of metal oxides [30, 33], which is consistent with our experimental results in present study.

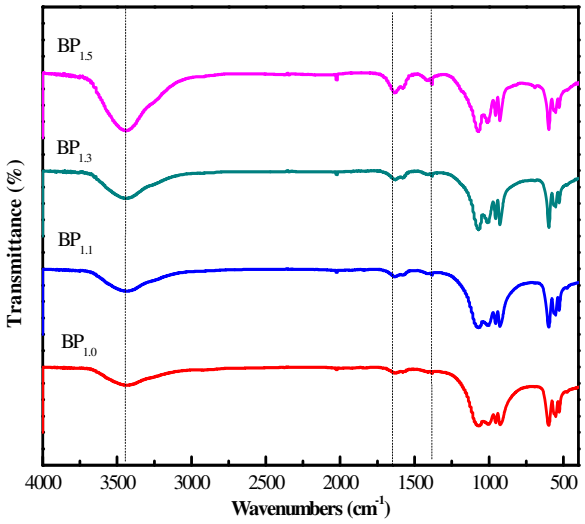

Fig. 4. FTIR spectra of the as-prepared bare $BiPO_4$ and phosphate-modified $BiPO_4$ samples.

3.5 XPS

XPS was performed to identify the chemical states of various elements in the as-prepared bare $BiPO_4$ and phosphate-modified $BiPO_4$ samples. Figure 5a shows the survey spectra of the products, where Bi, O, P, and C were detected in all the samples. The C 1*s* region with the binding energy at 284.8 eV in Figure 5b can be ascribed to the adventitious hydrocarbon; this spectrum was used as the reference standard. The high-resolution XPS spectra of Bi 4*f*, P 2*p* and O 1*s* on the surface of the samples are shown in Figures 3d–3e, respectively.

In Figure 5c, the Bi 4*f* spectra of all the samples were characterized by a Bi $4f_{5/2}$ peak at approximately 165.1 eV and a Bi $4f_{7/2}$ peak at 159.7 eV, which both belong to Bi^{3+} in $BiPO_4$ [42, 43]. The XPS spectra in the P 2*p* region (Figure 5d) exhibited a broad signal peak at approximately 133.3 eV, which corresponded to P (+5) in PO_4^{3-} [11]. The O 1*s* spectra in Figure 5e can be fitted by three peaks at 529.8, 530.5, and 531.5 eV, which correspond to the Bi-O, P-O, and OH groups, respectively [39, 44]. Interestingly, the binding energy of Bi 4*f*, P 2*p*, and O 1*s* shifted to a lower energy as the P/Bi ratio increased from 1.0 to 1.3, thereby indicating that the electron density

increased after the phosphate modification reached a P/Bi ratio of 1.3. As we all know, PO_4^{3-} groups possess a large electron cloud overlapping with high negative charges. Thus, the increased electron density is inferred to be caused by aggrandized PO_4^{3-} on the surface of $BiPO_4$. Furthermore, PO_4^{3-} has the induced effect that the dipole moment induces the formation of local fields preferring to attract holes and repel electrons, which helps the e^-/h^+ separation and benefits for the photocatalytic performance. The surface phosphate concentration becomes saturated when the P/Bi ratio exceeds 1.3, which is consistent with the FTIR results. The combined XPS spectra and IR results imply that the excess PO_4^{3-} was modified on the surface of $BiPO_4$.

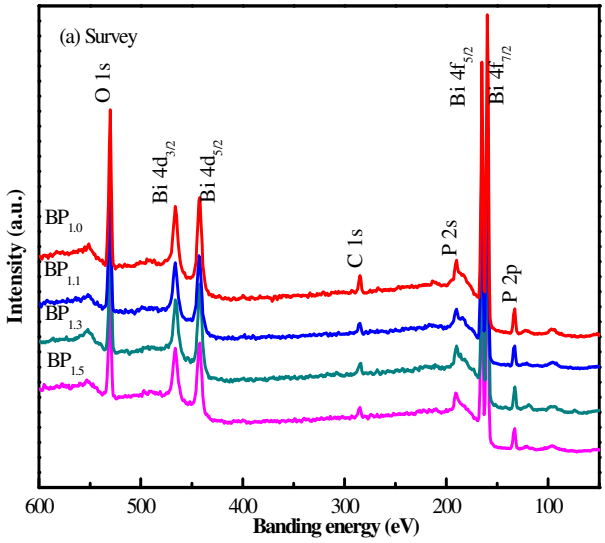

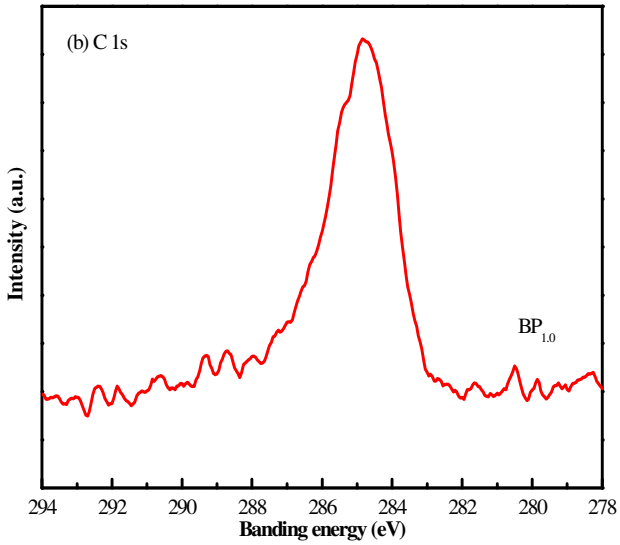

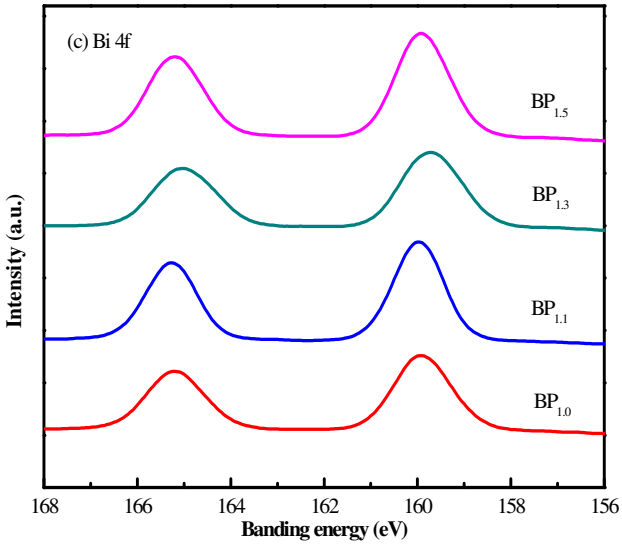

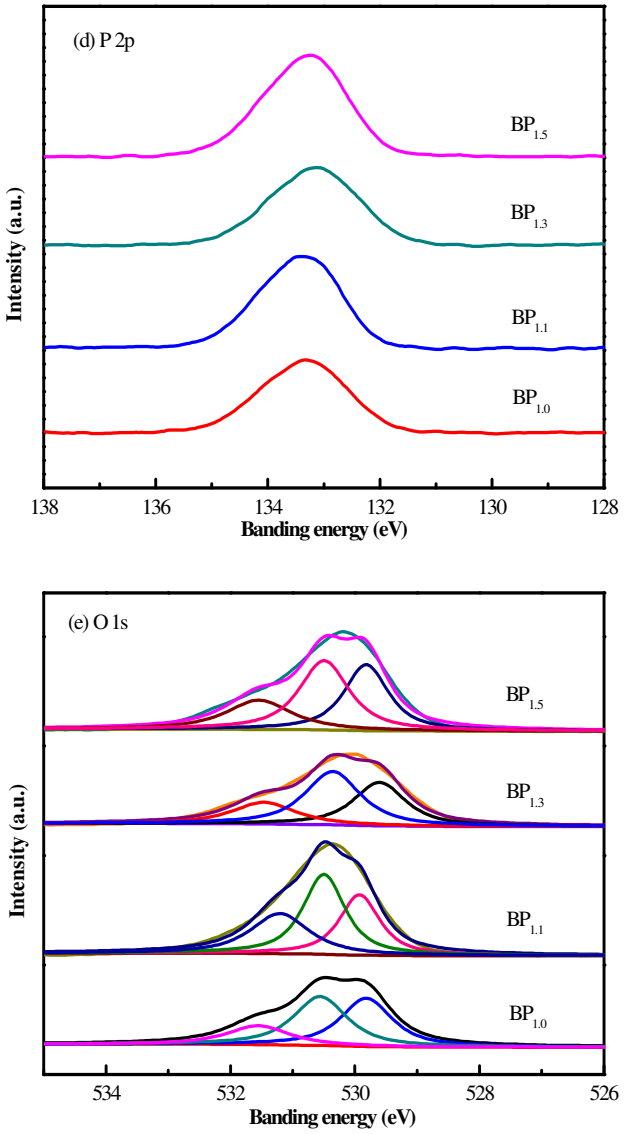

Fig. 5. High-resolution XPS spectra of the as-prepared $BiPO_4$: (a) Survey, (b) C 1s, (c) Bi 4f, (d) P 2p and (e) O 1s.

3.6 UV-vis diffuse reflectance spectra (DRS)

Figure 6 shows the typical UV-vis DRS of the as-prepared surface-modified and unmodified $BiPO_4$ samples. UV-vis DRS is normally used to characterize the electronic states of a semiconductor photocatalyst, wherein the electronic structure has a crucial role in the photocatalytic activity. As displayed in Figure 6, all the $BiPO_4$ products showed significant photo-absorption at wavelengths shorter than 300 nm,

which is consistent with previously published results [13]. Moreover, an obvious blue shift by several nanometers in the band gap transition appeared for the phosphate-modified $BiPO_4$ samples compared with the $BP_{1.0}$ sample. This change indicates that the band gap of the phosphate-modified $BiPO_4$ is larger than that of the $BP_{1.0}$ sample. The steep shape of the spectrum indicated that the UV light absorption was caused by the band gap transition rather than the transition from the impurity to the conduction band (CB). By assuming that $BiPO_4$ is an indirect semiconductor [4], the band gap energies of surface-modified $BiPO_4$ samples estimated from the $(\alpha h\nu)^{1/2}$ versus photon energy ($h\nu$) plots were 3.92, 3.95, 4.09, and 4.18 eV for $BP_{1.0}$, $BP_{1.1}$, $BP_{1.3}$, and $BP_{1.5}$, respectively (inset of Figure 6). This trend indicates that the surface-modification by PO_4^{3-} can enlarge the band gap of $BiPO_4$. This effect was probably caused by the morphological and particle size changes of the products after PO_4^{3-} introduction during the synthesis processes.

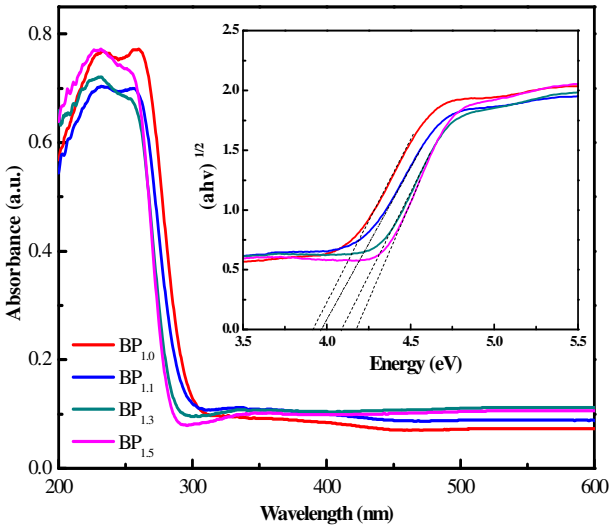

Fig. 6. UV-vis absorption spectra of the as-prepared phosphate-modified $BiPO_4$ samples (with P/Bi ratios varying from 1.0 to 1.5). The inset show plots of $(\alpha h\nu)^{1/2}$ versus photon energy ($h\nu$), where α is the absorption coefficient.

3.7 BET

Furthermore, the BET surface area of the as-prepared samples grew larger, but the

pore diameters became smaller with increased PO_4^{3-}/Bi^{3+} molar ratio (Table 1). These changes may be caused by the altered morphologies and sizes of $BiPO_4$. Notably, the changes in the total pore volume were not caused by the stable structures of the as-prepared $BiPO_4$. Therefore, the excess PO_4^{3-} can slightly increase the surface area of $BiPO_4$.

Table 1. Summary of surface area, total pore volume and pore diameter of the as-prepared $BiPO_4$.

Sample	S_{BET} (m^2/g)	Total pore volume (cm^3/g)	Pore diameter (nm)
$BP_{1.0}$	1.3008	0.00477	14.665
$BP_{1.1}$	1.1243	0.00635	22.596
$BP_{1.3}$	2.9507	0.00565	7.6636
$BP_{1.5}$	4.1968	0.00664	6.33

3.8 PL

PL emission is a useful technique for investigating the generation, transfer, and recombination of charge carriers. A low PL intensity has been proven to be generally indicative of a high separation efficiency of electron–hole pairs [45]. The PL spectra of $BP_{1.0}$ and $BP_{1.3}$ from Figure 7 exhibited a broad emission peak centered at approximately 275–475 nm [17]. $BP_{1.3}$ showed significantly diminished PL intensity compared with $BP_{1.0}$, which suggests that the modification of PO_4^{3-} on the surface of $BiPO_4$ results in a remarkable decline in the recombination rate of electron–hole pairs. This result is supported by the fact that hydroxyl on the surface can function as a hole trap and contribute to electron–hole separation.

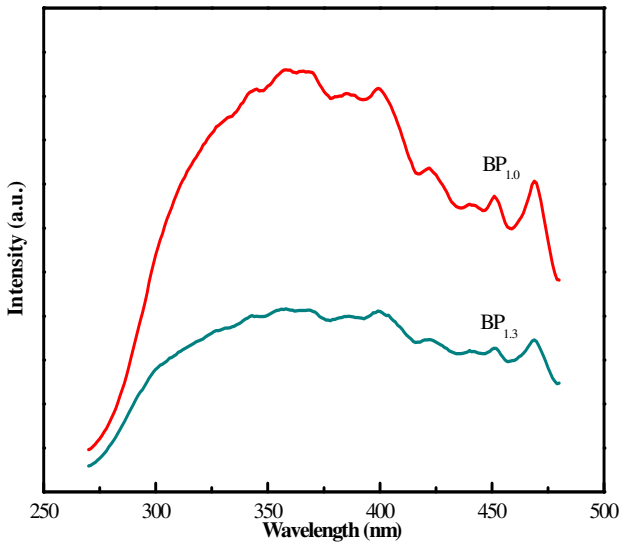

Fig. 7. PL spectra of $BP_{1.0}$ and $BP_{1.3}$.

3.9 Photoelectrochemical property

From Figure 8, it can be seen that the photocurrent was drastically increased when the irradiation was turned on, whereas the photocurrent value rapidly decreased to zero as soon as the irradiation was turned off. The measured photocurrent density of $BP_{1.3}$ (about 4.2 μA/cm^2) was significantly larger than that of $BP_{1.0}$ (1.3 μA/cm^2). This enhanced photocurrent indicated that the PO_4^{3-} modification for $BiPO_4$ could efficiently improve the separation of photogenerated electron-hole pairs.

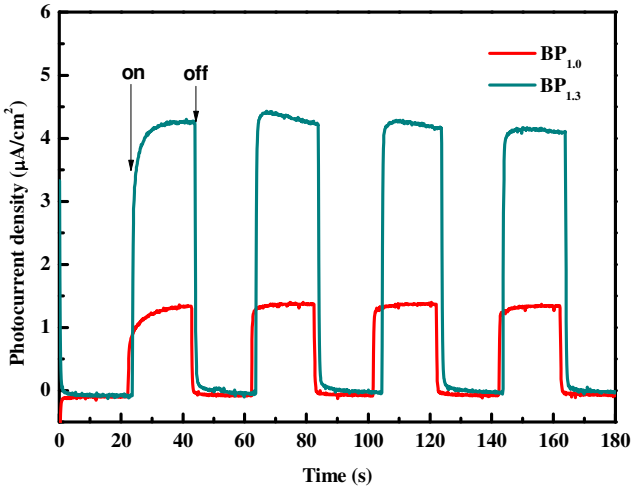

Fig. 8. Photocurrent transient with light on/off every 20 s for 180 s for $BP_{1.0}$ and

$BP_{1.3}$.

3.10 Photocatalytic activity

The photocatalytic activity of the as-prepared samples was evaluated by the decomposition of MO under UV light and simulated solar-light irradiation, respectively. As shown in Figure 9, the degradation efficiency of MO without photocatalysts was less than 10%. After the $BiPO_4$ surface was modified by different amounts of PO_4^{3-}, the photocatalytic performance of the modified samples was significantly improved. For example, under UV light irradiation, the MO was degraded by approximately 80% of the original unmodified $BiPO_4$ sample after an hour of the reaction. By contrast, the same amount was completed destroyed by phosphate-modified $BiPO_4$ photocatalysts under identical conditions. Moreover, the $BP_{1.3}$ and $BP_{1.5}$ samples show much superior activity than $BP_{1.1}$, which is much more significant for the photocatalytic performance under simulated solar-light irradiation (Figure 9b). These results indicated that the photocatalytic activities of the as-prepared products were significantly enhanced with the surface modification by PO_4^{3-}. Interestingly, further increase in the PO_4^{3-} concentration (when the P/Bi ratio was over 1.3) in the synthetic system had an insignificant influence on the photocatalytic activity improvement of $BiPO_4$. This trend may be attributed to the surface of bare $BiPO_4$, which was completely occupied by PO_4^{3-} at a P/Bi ratio of 1.3.

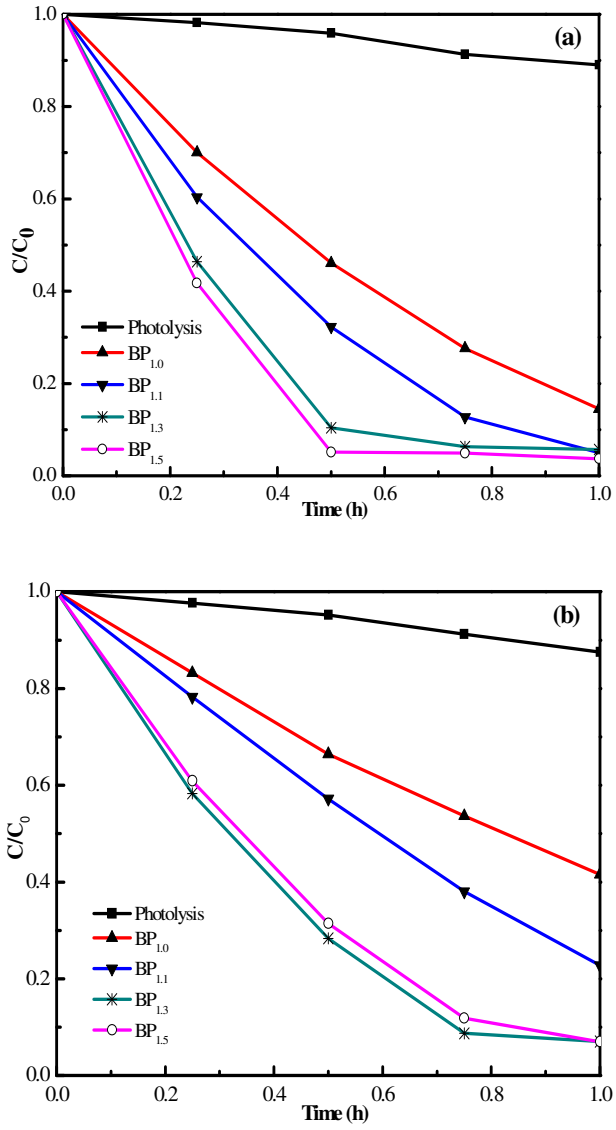

Fig. 9. Photocatalytic activity of the as-prepared phosphate-modified $BiPO_4$ samples for the degradation of MO under UV light (a) and simulated solar light (b) irradiation, respectively.

3.11 Reaction pathways for the photocatalytic degradation of MO with phosphate-modified $BiPO_4$ samples

During the photocatalytic degradation reactions in aqueous solutions, oxidative species including hydroxyl free radicals (•OH), holes (h^+), and free oxygen radicals

($\bullet O_2^-$) played an important role in the mineralization of pollutants. Different scavengers were added to the reaction systems to determine which species had a major role on the degradation of MO under simulated solar-light irradiation. As shown in Figure 10, the MO degradation rate and efficiency of $BP_{1.3}$ were significantly reduced after adding isopropyl alcohol (scavenger of •OH) to the degradation system; thus, the removal efficiency was reduced from 90% to 40%. However, by adding ammonium oxalate (scavenger of h^+) and ascorbic acid (scavenger of $\bullet O_2^-$) to the degradation system, the MO removal rates and efficiencies were slightly suppressed. These experimental results indicated that oxidation by •OH is the dominant reaction pathway for MO removal with phosphate-modified $BiPO_4$ samples, whereas holes and free oxygen radicals do not have significant roles in MO mineralization.

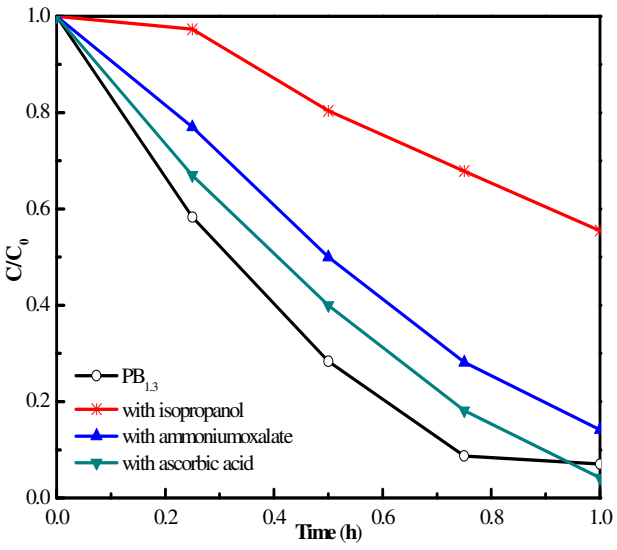

Fig. 10. Variations of MO photocatalytic removal efficiencies over a $BP_{1.3}$ sample with and without the addition of radical scavengers under simulated solar-light irradiation.

Aside from the above-mentioned indirect scavenger method, the ESR method was also adopted for the direct determination of the production and intensity of free radicals, with DMPO as the spin-trap reagent during the photocatalytic degradation

processes under ultraviolet light irradiation with wavelength of 245 nm. As presented in Figure 11a, no signals of •OH radicals were detected for the surface-modified and bare $BiPO_4$ photocatalysts (i.e., samples $BP_{1.0}$ and $BP_{1.3}$) before simulated UV light irradiation. Meanwhile, the four characteristic peaks of DMPO–•OH with an intensity ratio of 1:2:2:1 were observed after 30 min of irradiation which suggested the generation of OH radicals during the photocatalytic degradation processes [46]. Moreover, the intensity of DMPO–•OH signals with $BP_{1.3}$ was much higher than those with $BP_{1.0}$, thereby demonstrating that the phosphate modification can facilitate the generation of OH radicals during degradation. This result can probably be ascribed to the presence of a large amount of hydroxyl groups adsorbed on the surface of $BP_{1.3}$ as compared with the bare $BiPO_4$. These groups can facilitate the separation of photogenerated charge carriers and eventually enhance the photocatalytic activity. Moreover, no free oxygen radicals ($•O_2^-$) were detected by ESR methods, as shown in Figure 11b, thereby indicating that MO was predominantly removed via oxidation by •OH radicals.

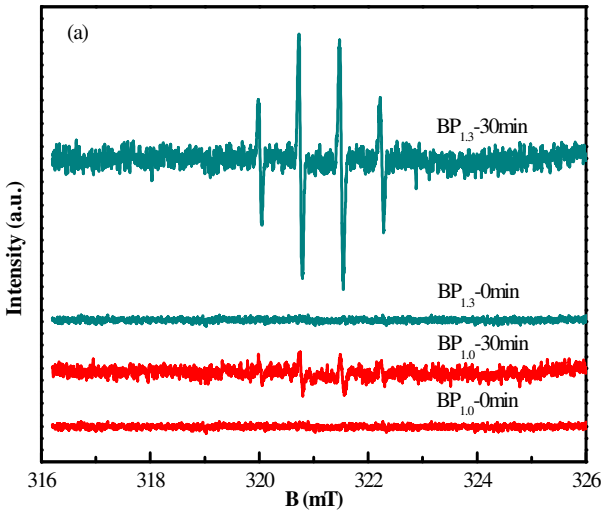

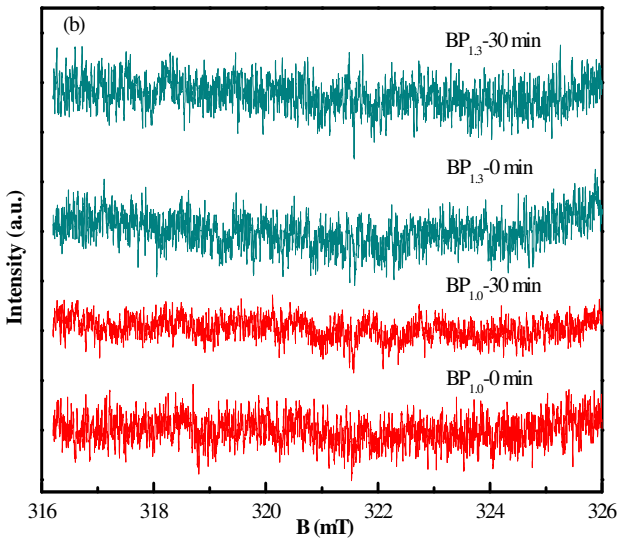

Fig. 11. DMPO spin-trapping ESR spectra under simulated solar-light irradiation for 0 and 30 min at room temperature of water (a) and ethanol (b) in the presence of $BP_{1.0}$ and $BP_{1.3}$, respectively.

Theoretically, the band positions of $BiPO_4$ can be calculated by the following empirical equations:

$$E_{VB} = X - E^e + 0.5E_g \quad (1)$$

$$E_{CB} = E_{VB} - E_g \quad (2)$$

Where E_{VB} is the VB edge potential and E_{CB} is the CB edge potential. X is the electro-negativity of the semiconductor, which is the geometric mean of the electro-negativity of the constituent atoms, and the value of X for $BiPO_4$ is 6.49 eV. E^e is the energy of free electrons on the hydrogen scale (approximately 4.5 eV), whereas E_g is the band gap energy of the semiconductor photocatalyst [47]. Based on the band gap energies calculated from the UV-vis DRS characterization results, the VB edge potentials of the as-prepared bare $BiPO_4$, $BP_{1.1}$, $BP_{1.3}$, and $BP_{1.5}$ samples are 3.89, 4.00, 4.05, and 4.09 eV, respectively. Meanwhile, the CB edge potentials of the corresponding bare $BiPO_4$, $BP_{1.1}$, $BP_{1.3}$, and $BP_{1.5}$ samples are 0.09, -0.02, -0.05, and -0.11 eV, respectively. Given that the redox potential of $O_2/\bullet O_2^-$ is -0.33 eV, which is more negative than the CB edge potentials of all the as-prepared $BiPO_4$ samples, the

CB electrons could not reduce O_2 to $\bullet O_2^-$. Meanwhile, the potentials of the holes at the VB of all the as-prepared $BiPO_4$ are more positive than that of $OH^-/\bullet OH$ (1.99 eV); thus, the holes can oxidize OH^- into •OH radicals [16]. These theoretical calculation results confirm the active species identification results from the scavenger and direct ESR methods.

Therefore, based on the characterization results, we proposed a photocatalytic degradation mechanism of MO over the as-prepared phosphate-modified $BiPO_4$ as shown in Figure 12. From the FTIR and XPS characterization results, the surface modification of $BiPO_4$ by PO_4^{3-} can enhance the surface hydroxyl group concentration and improve its hydrophilic property. The concentration of PO_4^{3-} adsorbed on the surfaces of the as-prepared samples would be saturated when the molar ratio of PO_4^{3-}/Bi^{3+} exceeds 1.3, thereby preventing further photocatalytic activity improvement. Compared with bare $BiPO_4$, the phosphate-modified $BiPO_4$ samples facilitated the separation of photogenerated electrons and holes under simulated solar-light irradiation because of the improved hydrophilic properties, which eventually enhanced MO degradation efficiency. Moreover, as depicted in Figure 12, when the catalyst was irradiated with simulated solar light, excited electrons transferred from the VB to the CB. The holes left in VB could act with hydroxyl to form hydroxyl free radicals because of its suitable electrode potential position, thereby leading to the effective separation of photo-generated carriers. However, the electrons in CB were unable to reduce oxygen to $\bullet O_2^-$ because of its much more positive reduction potential. Therefore, the experimental and theoretical results evidenced that •OH is the predominant active species for MO degradation in the reaction system.

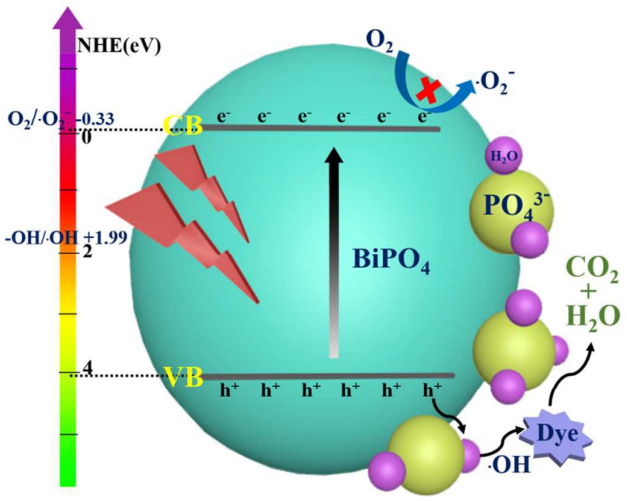

Fig. 12. Schematic diagram of the photocatalytic degradation mechanism of MO with the as-prepared phosphate-modified $BiPO_4$ samples under simulated solar-light irradiation.

4. Conclusion

Surface modification by phosphate can efficiently improve the photocatalytic performance of $BiPO_4$ for the degradation of MO, which can be ascribed to the high crystallinity, uniform morphology, and increased surface OH concentrations of the phosphate-modified $BiPO_4$ samples. According to the characterization results, PO_4^{3-} modification can facilitate the separation of photo-excited electrons and holes. The produced OH radicals were identified as the dominant active species for MO oxidation in the photocatalytic degradation system, rather than via the reaction with O_2^- radicals. Therefore, PO_4^{3-} modification is an effective method for improving the activity of $BiPO_4$.

Acknowledgements

This research was financially supported by the National Science Foundation of China (21303116, 41401567, 41573138), Shanxi Province Science Foundation (2013021011-2) and partially supported by the Research Grants Council of Hong

Kong (PolyU 152083/14E), a research grant of the Early Career Scheme (ECS 809813) from the Research Grant Council, the Hong Kong SAR Government, the Dean's Research Fund-Early Career Researchers (04022), the Research Equipment Grant (REG-2), and the Internal Research Grant (R3429) from The Hong Kong Institute of Education.

References

[1] C. C. Chen, W. H. Ma and J. C. Zhao, *Chem. Soc. Rev.*, 2010, **39**, 4206.

[2] C. S. Pan, J. Xu, Y. Chen and Y. F. Zhu, *Appl. Catal. B*, 2012, **115-116**, 314.

[3] L. Körösi, S. Papp, I. Bertóti and I. Dékány, *Chem. Mater.*, 2007, **19**, 4811.

[4] C. S. Pan and Y. F. Zhu, *Environ. Sci. Technol.*, 2010, **44**, 5570.

[5] N. Zhang, M. Q. Yang, S. Q. Sun and Y. J. Xu, Chem. Rev., 2015, 115, 10307.

[6] M. Q. Yang, N. Zhang, M. Pagliaro and Y. J. Xu, Chem. Soc. Rev., 2014, 43, 8240.

[7] S. Q. Liu, Z. R. Tang, Y. G. Sun, J. C. Colmenares and Y. J. Xu, Chem. Soc. Rev., 2015, 44, 5053.

[8] T. Lv, L. K. Pan, X. J. Liu and Z. Sun, *RSC Adv.*, 2012, **2**, 12706.

[9] J. Cao, B. Y. Xu, H. L. Lin and S. F. Chen, *Chem. Eng. J.*, 2013, **228**, 482.

[10] H. L. Lin, H. F. Ye, B. Y. Xu, J. Cao and S.F. Chen, *Catal. Commun.*, 2013, **37**, 55.

[11] M. H. Fulekar, A. Singh, D. P. Dutta, M. Roy, A. Ballal and A. K. Tyagi, *RSC Adv.*, 2014, **4**, 10097.

[12] Y. H. Lv, K. Huang, W. Zhang, B. Yang, F. L. Chi, S. L. Ran and X. G. Liu, *Ceram. Int.*, 2014, **40**, 8087.

[13] C. S. Pan and Y. F. Zhu, *J. Mater. Chem.*, 2011, **21**, 4235.

[14] C. S, Pan, D. Li, X. G. Ma, Y. Chen and Y. F. Zhu, *Catal. Sci. Technol.*, 2011, **1**, 1399.

[15] B. Lu, X. G. Ma, C. S. Pan and Y. F. Zhu, *Appl. Catal. A*, 2012, **435-436**, 93.

[16] Y. F. Liu, Y. Y. Zhu, J. Xu, X. J. Bai, R. L Zong and Y. F. Zhu, *Appl. Catal. B*, 2013, **142-143**, 561.

[17] Y. Y. Zhu, Y. F. Liu, Y. H. Lv, Q. Ling, D. Liu and Y. F. Zhu, *J. Mater. Chem. A*, 2014, **2**, 13041.

[18] B. H. Long, J. H. Huang and X. C. Wang, *Prog. Nat. Sci.*, 2012, **22**, 644.

[19] J. Xu, L. Li, C. S. Guo, Y. Zhang and W. Meng, *Appl. Catal. B*, 2013, **130-131**, 285.

[20] M. Ruwet, S. Ceckiewicz, and B. Delmon, *Ind. Eng. Chem. Res.*, 1987, **26**, 1981.

[21] Z. Holgye, *J. Radioanal. Nucl. Chem.*, 1998, **227**, 127.

[22] M. Sheng, L. L. Gu, R. Kontic, Y. Zhou, K. B. Zheng, G. R. Chen, X. L. Mo and G. R. Patzke, *Sens. Actuators B*, 2012, **166**, 642.

[23] C. S. Pan, J. Xu, Y. J. Wang, D. Li and Y. F. Zhu, *Adv. Funct. Mater.*, 2012, **22**, 1518.

[24] F. F. Duo, Y. W. Wang, X. M. Mao, X. C. Zhang, Y. F. Wang and C. M. Fan, *Appl. Surf. Sci.*, 2015, **340**, 35.

[25] Y. N. Zhang, H. Q. Fan, M. M. Li and H. L. Tian, *Dalton Trans.*, 2013, **42**, 13172.

[26] Y. F. Liu, Y. H. Lv, Y. Y. Zhu, D. Liu, R. L. Zong and Y. F. Zhu, *Appl. Catal. B*, 2014, **147**, 851.

[27] L. N. She, G. Q. Tan, H. J. Ren, J. Huang, C. Xu and A. Xia, *RSC Adv.*, 2015, **5,** 36642.

[28] Y. H. Lv, Y. Y. Zhu and Y. F. Zhu, *J. Phys. Chem. C*, 2013, **117**, 18520.

[29] Y. H. Lv, Y. F. Liu, Y. Y. Zhu and Y. F. Zhu, *J. Mater. Chem. A*, 2014, **2**, 1174.

[30] J. Huang, W. Liu, D. S. Dolzhnikov, L. Protesescu, M. V. Kovalenko, B. Koo, S. Chattopadhyay, E. V. Shenchenko and D. V. Talapin, *ACS Nano*, 2014, **8,** 9388.

[31] H. Q. Cui, Y. Cao, L. Q. Jing, Y. B. Luan and N. Li, *Chempluschem,* 2014*,* **79** 318.

[32] P. Mohapatra and K. M. Parida, *J. Mol. Catal. A: Chem.*, 2006, **258**, 118.

[33] D. Zhao, C. C. Chen, Y. F. Wang, H. W. Ji, W. H. Ma, L. Zang and J. C. Zhao, J.

Phys. Chem. C, 2008, **112**, 5993.

[34] L. M. He, L. Q. Jing, Z. J. Li, W. T. Sun and C. Liu, *RSC Adv.*, 2013, **3**, 7438.

[35] L. Q. Jing, J. Zhou, J. R. Durrant, J. W. Tang, D. N. Liu and H. Q. Fu, *Energy Environ. Sci.*, 2012, **5**, 6552.

[36] C. S. Pan and Y. F. Zhu, Catal. Sci. Technol., 2015, 5, 3071.

[37] G. H. Tian, H. G. Fu, L. Q. Jing and C. G. Tian, *J. Hazard. Mater.*, 2009, **161**, 1122.

[38] A. Bhaumik and S. Inagaki, *J. Am. Chem. Soc.*, 2001, **123**, 691.

[39]J. Jiménez-Jiménez, P. Maireles-Torres, P. Olivera-Pastor, E. Rodríguez-Castellón, A. Jiménez-López, D. J. Jones and J. Rozière, *Adv. Mater.*, 1998, **10**, 812.

[40] J. C. Yu, L. Z. Zhang, Z. Zheng and J. C. Zhao, *Chem. Mater.*, 2003, **15**, 2280.

[41] X. Qin, L. Q. Jing, G. H. Tian, Y. C. Qu and Y. J. Feng, *J. Hazard. Mater.*, 2009, **172**, 1168.

[42] H. Xu, Y. G. Xu, H. M. Li, J. Xia, J. X. Xiong, S. Yin, C. J. Huang and H. L. Wan, *Dalton Trans.*, 2012, **41**, 3387.

[43] S. Y. Wu, H. Zheng, Y. W. Lian and Y. Y. Wu, *Mater. Res. Bull.*, 2013, **48**, 2901.

[44] H. L. Lin, H. F. Ye, X. Li, J. Cao and S. F. Chen, *Ceram. Int.*, 2014, **40**, 9743.

[45] F. Dong, Q. Y. Li, Y. J. Sun and W. K. Ho, *ACS Catal.*, 2014, **4**, 4341.

[46] C. M. Arroyo, J. H. Kramer, B. F. Dickens and W. B. Weglicki, *FEBS Lett.*, 1987, **221**, 101.

[47] X. Lin, D. Liu, X. Y. Guo, N. Sun, S. Zhao, L. M. Chang, H. J. Zhai and Q. W. Wang, *J. Phys. Chem. Solids*, 2015, **76**, 170.